Chinese Journal of Catalysis 38 (2017) 1443–1453 催化学报 2017年 第38卷 第9期 | www.cjcatal.org

available at www.sciencedirect.com

ScienceDirect

journal homepage: www.elsevier.com/locate/chnjc

Perspective (Special Issue of the International Symposium on Single-Atom Catalysis (ISSAC-2016))

Two-dimensional materials confining single atoms for catalysis

Yong Wang [a,c], Wenhua Zhang [b], Dehui Deng [a,c,*], Xinhe Bao [a,#]

1. Introduction

Single atoms that act as catalysts are widely found in nature and play important roles in vital molecules, e.g., Mo in nitrogenase [1], Fe in heme [2], and Mg in chlorophylls [3]. In vivo, single atoms that act as catalysts are coordinated with biomacromolecules and work cooperatively. Similarly, synthetic chemical ligands can provide single atoms in biomimetic functions and other applications. For example, Wilkinson's catalyst ($RhCl[P(C_6H_6)_3]_3$), the first successful homogeneous catalyst, is commonly used for hydrogenation, hydroformylation, hydrosilylation, and hydroboration of alkenes and alkynes. Such homogeneous catalysts usually have excellent catalytic turnover numbers because they take full advantage of each metal atom, but the instability of these organic molecular ligands and the difficulty of catalyst recovery are major drawbacks. Inorganic solid materials can also serve as specific ligands for single metal atoms [4], and the concept of single-site [5,6] or single-atom catalysts (SACs) [7,8] is being increasingly developed [8–12]. Among heterogeneous supports, traditional bulk metal oxides, e.g., MgO, Al_2O_3, SiO_2, TiO_2, FeO_x, ZnO, and CeO_2, zeolites, and metal-organic frameworks are generally used to stabilize various single metal atoms [9]. The excellent catalytic performance of a SAC arises from both the coordinatively unsaturated state of the active center and its stable coordination with the support. Two-dimensional (2D) materials with special physical and chemical properties could therefore provide a new class of promising and ideal supports for single atoms, but this has not been widely studied.

The successful exfoliation of graphene [13] has led to an increase in the use of 2D materials, and the use of analogous materials such as *h*-NB, C_3N_4, and MoS_2 is expanding [14–16]. These 2D materials are not only excellent catalysts in themselves [17] but also have may specific advantages in constructing SACs. First, 2D materials with unique geometric and electronic structures [17] can modulate the catalytic behavior of single atoms in unusual ways. Secondly, 2D materials always have large specific surface areas, which can create more active sites by anchoring single atoms on the surface. Thirdly, strictly single-atom-layer 2D materials can facilitate the adsorption and diffusion of reactive molecules on confined single atoms from two sides. Fourthly, such composites provide model catalysts for which uniformly active sites can be well identified and catalytic performances can be predicted using theoretical chemical methods [18]. Finally, the confined single atoms can promote or activate the intrinsic catalytic activities of 2D materials.

In this perspective, we summarize recent progress in research on catalysts based on the confinement of single atoms in 2D materials, mainly graphene, C_3N_4, and MoS_2. We focus on how 2D materials and confined single atoms work cooperatively in catalysis, the identity of the real active sites, and the potential practical applications of such novel catalysts.

2. Single atoms confined in graphene

Graphene consists of single-atom-layer sp^2 carbon, and can be easily doped with non-metal heteroatoms such as N, B, P, and S. Heteroatom-doped graphene materials are widely used in electrocatalysis [19] and photocatalysis [20]. The N-doped graphenes have been widely researched and various methods for their preparation by direct synthesis or post-treatment synthesis have been developed [21]. Doping of N into the graphene lattice polarizes the carbon network, which changes the electronic properties of graphene. This N-induced electronic perturbation can be directly observed using scanning tunneling microscopy (STM) [22,23]. Deng *et al*. reported that the STM images of N-doped graphenes show brighter sections that are distinct from the main graphene network (Fig. 1(a) and (b)); this has also been observed in other studies (Fig. 1(c)). These observations indicate substitution of N atoms in graphene. Density functional theory (DFT) calculations and STM simulations have confirmed that these bright spots are not images of N atoms but of C atoms neighboring N atoms, and are the result of increased electron densities of states caused by doping with N atoms [22,23]. Such doped graphitic N single atoms (Fig. 1) not only facilitate the dissociation of O_2 molecules on adjacent C atoms but also promote the formation of strong C–O chemical bonds through electronic interactions. The catalytic activity of N-doped graphene is therefore better than those of pure graphene and commercial XC-72 in oxygen reduction reactions (ORRs) [22].

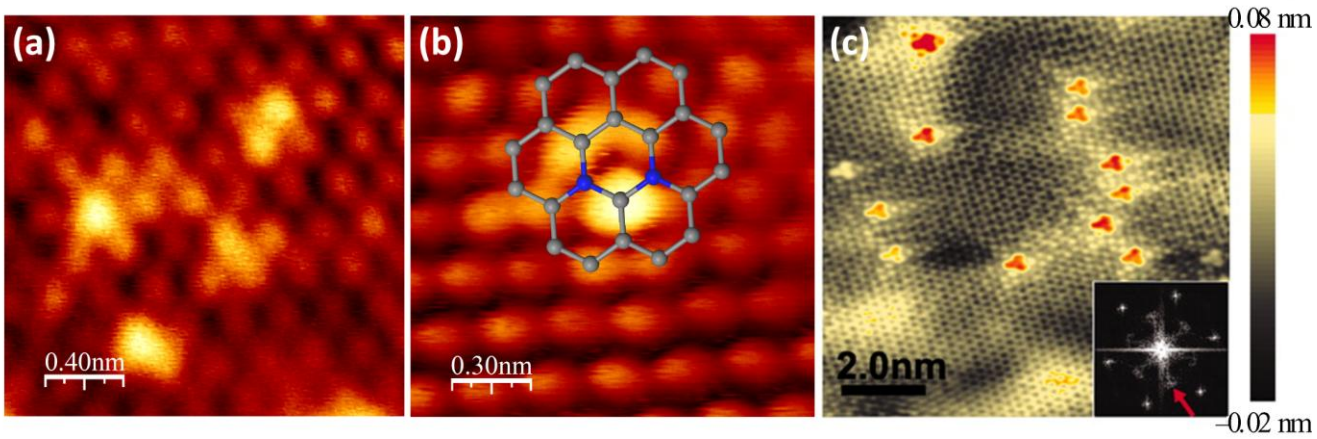

Fig. 1. STM images of N-doped graphene. (a,b) High-resolution images obtained at V_{bias} = 0.5 V, I_{set} = 53.4 pA, and V_{bias} = 0.9 V, I_{set} = 104 pA, respectively [22]; (c) Image of ~14 graphitic N dopant atoms with inset showing FFT topography (V_{bias} = 0.8 V, I_{set} = 0.8 nA) [23].

Research on graphene-confined SACs has increased recently because of their broad range of applications. Sun *et al.* used atomic layer deposition (ALD) to anchor Pt single atoms on graphene [24] or on N-doped graphene [25,26], and these Pt SACs were used in the electrocatalytic methanol oxidation reaction (MOR) [24], ORR [25], and hydrogen evolution reaction (HER) [26]. The activities of Pt SACs are 10 times and 37 times higher than those of their Pt nanoparticle (NP) counterparts (commercial Pt/C) in the MOR and HER, respectively. Based on DFT calculations and X-ray absorption fine structure (XAFS) analysis, the authors proposed that the low-coordination and partly unoccupied densities of states of the 5*d* orbitals of the Pt single atoms are responsible for the observed excellent catalytic performances [24,26]. Pt SACs also showed much higher CO tolerance during the MOR [24] and long-term stability (1000 cycles) during the HER [26]. This is attributed to the high binding energy between Pt single atoms and C (or O) atoms at the graphene edges [27], which can be enhanced by doping with N [25].

Similarly, Yan *et al.* [28] synthesized a Pd_1/graphene SAC using atomic layer deposition. In the selective hydrogenation of 1,3-butadiene, Pd_1/graphene showed about 100% selectivity for butenes (70% selectivity for 1-butene) at 95% conversion at 50 °C. Under the same conditions, graphene-supported Pd NPs (5.5 nm) gave only 70% selectivity for butenes and 15% selectivity for 1-butene. The authors suggested that changes in the 1,3-butadiene adsorption mode and enhanced steric effects at Pd single atoms are possible reasons for these results (Fig. 2(a)). Similar to the situation for graphene-supported Pt SACs [24–26], XAFS analysis indicated that Pd single atoms coordinate with defective C and phenolic O atoms (Fig. 2(a)) and therefore show +2 valence state behavior [28]. Such strong bonding interactions endow Pd_1/graphene with excellent durability against metal sintering and carbon deposition for a total 100 h of reaction time on stream [28].

Qiu *et al.* [29] used chemical vapor deposition to grow graphene on nanoporous Ni substrates. Three-dimensional (3D) graphene-confined Ni SACs can be acquired by subsequent acid etching, and can therefore be used for HERs in acidic solutions (0.5 mol/L of H_2SO_4). The overpotential (50 mV) and Tafel slope (45 mV/dec) for Ni SACs were lower than those for conventional Ni-based catalysts. It is proposed that the unusual catalytic performance of Ni_1/graphene is the result of *sp-d* orbital charge transfer between the Ni single atoms and the surrounding carbon atoms. Unlike Pt_1/graphene [24–26] and Pd_1/graphene [28], in which the single metal atoms are mainly anchored on graphene vacancies, a single Ni atom substitutes for one C atom in the graphene lattice and chemically bonds with three C atoms (Fig. 2(b)). DFT calculations show that graphene with substituted Ni atoms should be more efficient in the HER (Fig. 2(b)) [29], and the formed C–Ni bonds ensure excellent cycling stability (1000 cycles).

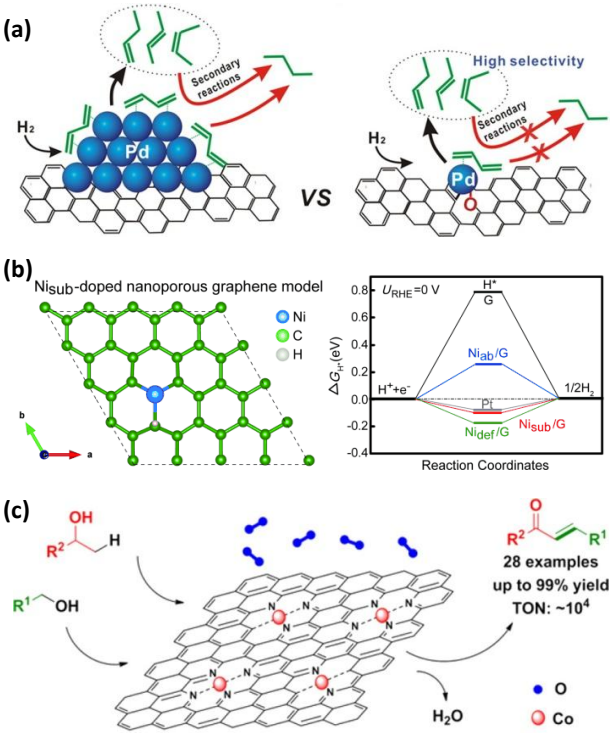

Fig. 2. Three anchoring modes of single metal atoms on graphene. (a) Pd single atom located at graphene defect for selective hydrogenation of 1,3-butadiene [28]; (b) Ni single atom substituting one C atom in graphene lattice for HER [29]; (c) Co single atoms coordinated with pyridinic N atoms in graphene matrix for C–C coupling reactions [30].

Co SACs confined in N-doped graphene for HERs have also been reported [31]. An overpotential of 30 mV was reached, and the durability was high (1000 cycles) under both acidic and basic conditions. The catalyst was prepared by simply heat-treating (750 °C) graphene oxide and cobalt salts in an Ar/NH_3 atmosphere. XAFS analysis indicated that Co single atoms strongly coordinate with N atoms, which are the catalytically active sites. However, the authors did not report the exact configuration. Zhang *et al*. [30] synthesized an analogous Co SAC using a similar pyrolysis method. They found that the active sites were Co–N–C structures with pyridinic N as coordinating atoms (Fig. 2(c)) in aerobic oxidative C–C coupling reactions, and the Co SAC showed the highest turnover frequency by far for these reactions. Furthermore, pyridinic N-stabilized single atoms of Pt-group metals [32,33] or base metals [34–36] were also reported to be the catalytically active sites in the decomposition of formic acid [32,33] or the ORR [34–36], respectively.

Although significant progress has been made in single-atom dispersed MN_x catalysts, their accurate synthesis and characterization are still a challenge [37]. Recently, Deng *et al*. [38] developed a facile ball-milling method for the large-scale synthesis of high-density and highly dispersed FeN_4 species confined in a graphene matrix. The atomic structure of FeN_4 centers in graphene were shown for the first time [38,39]. High-angle annular dark-field scanning transmission electron microscopy (HAADF-STEM) images (Fig. 3(a) and (b)) show homogeneously scattered Fe single atoms on graphene as small bright dots. The electron energy loss (EEL) atomic spectrum (Fig. 3(c)) of the bright dot in Fig. 3(b) clearly shows that the Fe and N atoms are adjacent to each other, suggesting the formation of Fe–N bonds. Low-temperature STM shows the atomic structure of the FeN_4 center embedded in the graphene matrix (Fig. 3(d)), which can also be well reconstructed using simulated STM (Fig. 3(e)). The Fe single atom is resolved as a bright spot, and the neighboring N and C atoms are brighter than the other C atoms in the graphene lattice, suggesting that the Fe single atom significantly modifies the densities of states of the adjacent atoms and vice versa. STM images across the FeN_4 center (Fig. 3(f)) show a sharp resonance state at −0.63 eV below the Fermi level, indicating that the Fe single atom strongly interacts with the graphene lattice and thus introduces a new electronic state near the Fermi level.

Such coordinatively unsaturated Fe sites (FeN_4/GN) are highly active in the catalytic oxidation of benzene to phenol at room temperature (Fig. 4(a)) and even at 0 °C because of the easy formation of Fe=O intermediates [38]. DFT calculations (Fig. 4(b)) showed that a H_2O_2 molecule can be easily dissociated on the FeN_4 center to form Fe=O and O=Fe=O intermediates successively; this is consistent with the XAFS analysis. The adsorption and activation of benzene on the O=Fe=O sites should be the rate determining step, with an energy barrier of

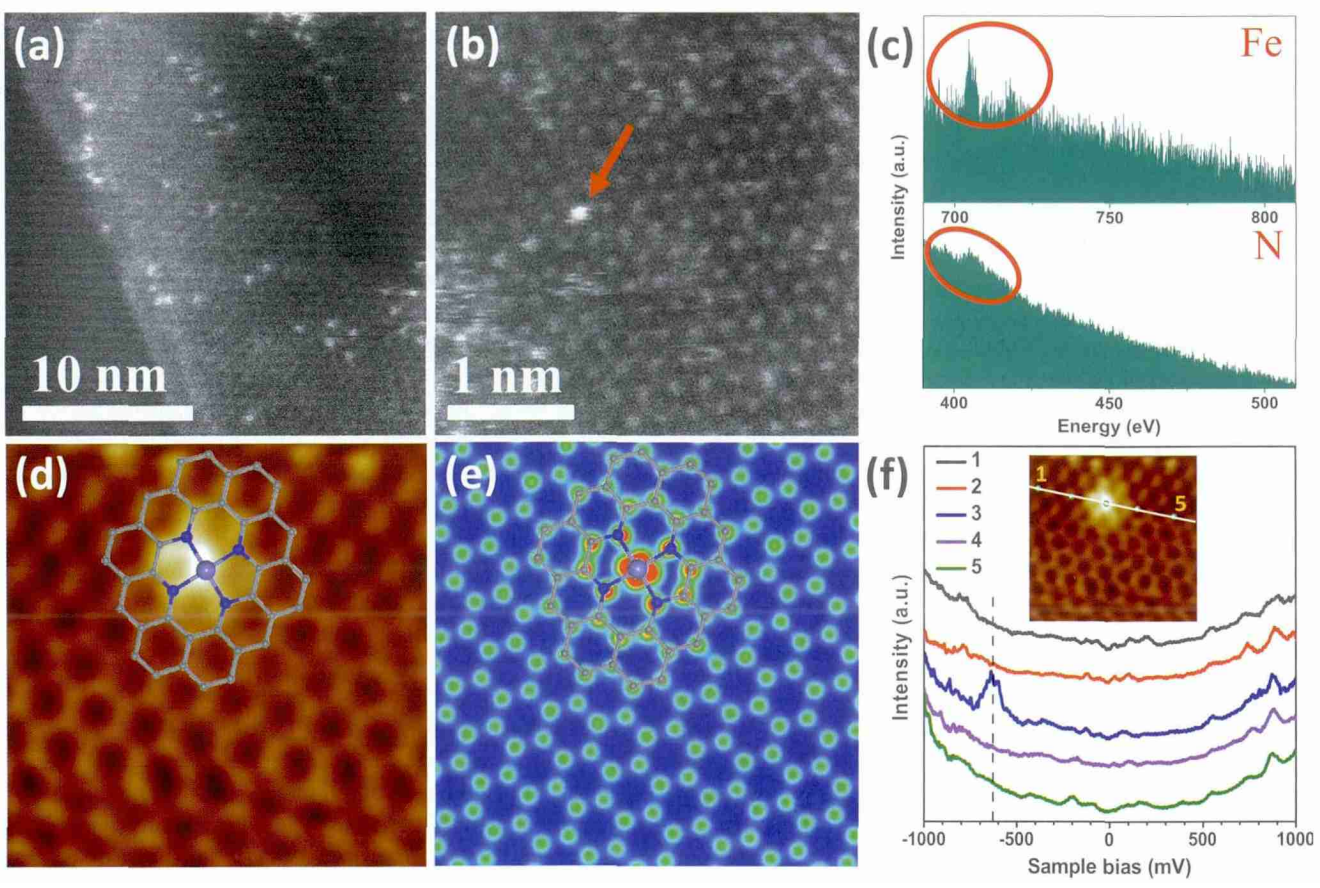

Fig. 3. Structural analysis of graphene-confined FeN_4 catalyst [38]. (a,b) HAADF-STEM images of graphene-confined FeN_4; (c) EEL atomic spectra of Fe and N elements from bright dots, shown by red arrow in (b); (d) Low-temperature STM image of graphene-confined FeN_4 (2 nm × 2 nm); (e) Simulated STM image for (d); (f) dI/dV spectra acquired along white line in inset image.

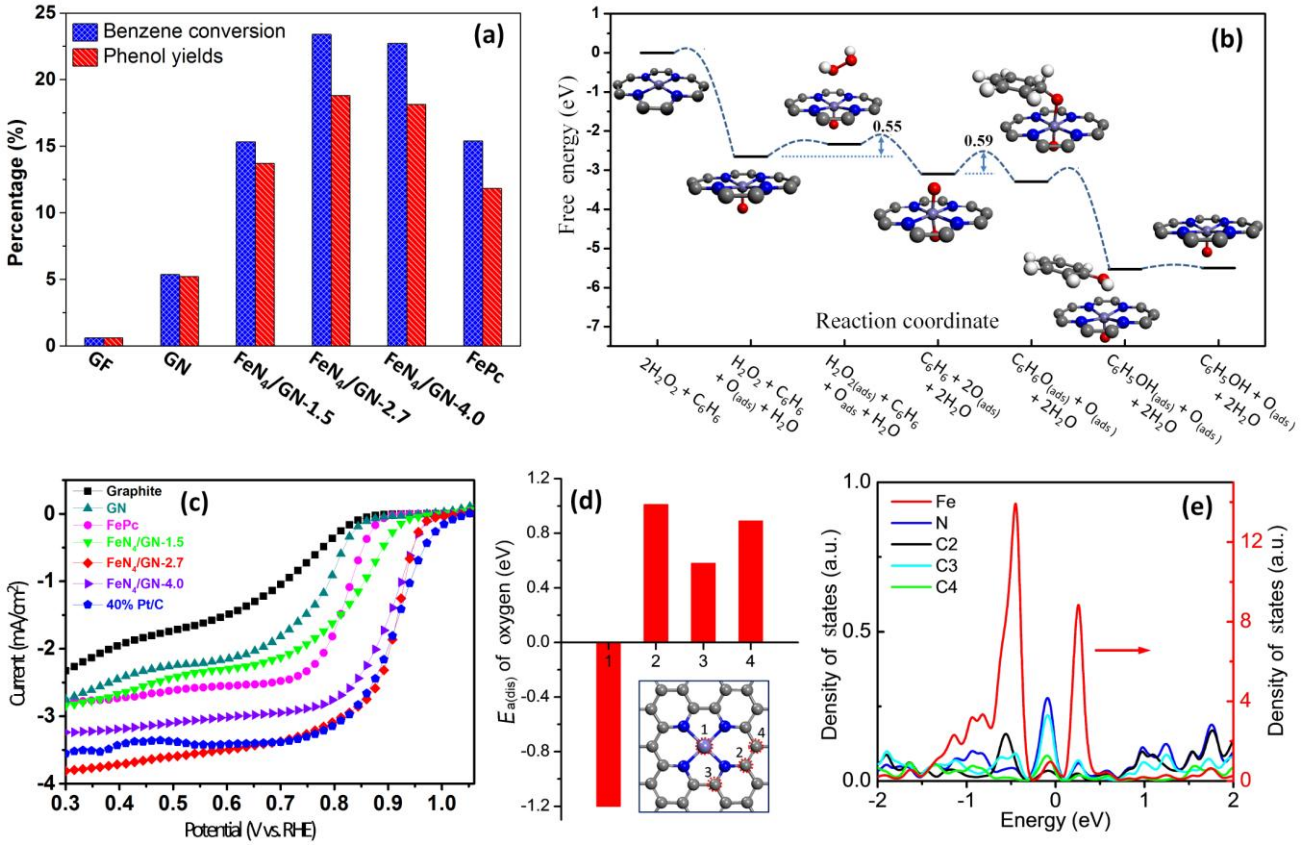

Fig. 4. Catalytic performances of FeN_4/GN catalyst. (a) Performance in benzene oxidation with H_2O_2 to phenol at room temperature [38]; (b) Free-energy diagram of benzene oxidation with H_2O_2 to phenol (gray, blue, light-blue, red, and white balls represent C, N, Fe, O, and H atoms, respectively) [38]; (c) ORR performance in O_2-saturated NaOH (1.0 mol/L) at scanning rate of 10 mV/s [40]; (d) Dissociative adsorption energy ($E_{a(dis)}$) of oxygen on different sites of graphene-confined FeN_4 structure, compared with gas-phase O_2 [40]; (e) Projected densities of states of Fe, N, and C atoms corresponding to inset in (d) [40].

only 0.59 eV, which is moderate and enables low-temperature reactions. Furthermore, the FeN_4 center can directly dissociate an O_2 molecule [40], and the dissociated O on the single Fe atom is much more strongly adsorbed than those on the C atoms (Fig. 4(d)) because of the notably higher distribution of the density of states of Fe near the Fermi level than of those of the C atoms (Fig. 4(e)). The ORR activity of FeN_4 SAC is therefore significantly high and comparable to that of commercial 40% Pt/C (Fig. 4(c)). FeN_4 SAC also has a higher stability and tolerances to SO_x, NO_x, and methanol than does Pt/C, probably because of its preferential adsorption of an O_2 molecule [40].

The high-energy ball-milling method [38] was used to synthesize various graphene-confined base-metal SACs with MN_4 (M = Mn, Fe, Co, Ni, or Cu) centers; the materials were used as counter electrodes in dye-sensitized solar cells (DSSCs) [41]. Among all these MN_4/GN catalysts, CoN_4/GN was the most active and stable in interconversion of the redox couple I^-/I_3^-, and its power conversion efficiency (PCE) surpassed that of a sputtered Pt electrode (Fig. 5(a)). DFT calculations showed that CoN_4/GN has superior properties because the adsorption energy of iodine on the confined Co sites is appropriate, leading to a good balance between adsorption and desorption processes (Fig. 5(c)). In detail (Fig. 5(b)), the optimum binding energy of iodine on MN_4, $E_{ad,I}$, is predicted to be about −0.80 eV, which exactly corresponds to that on CoN_4/GN. Furthermore, the confined CoN_4 structure is the most stable among these MN_4/GN catalysts because of the higher energy of Co–N bonds (inset in Fig. 5(b)). Both examples [40,41] show the potential of graphene-confined MN_4 SACs for replacing precious metals as catalysts.

The results described above show that graphene has various sites for confining single atoms, such as defective C or O, doped N, and even S [42], and these functional groups can modulate the catalytic performance of the SAC. A graphene-confined SAC usually shows high stabilities in many catalytic reactions, highlighting the potential for practical applications. The development of more efficient and facile methods for the large-scale production of graphene-confined SACs with high loadings is therefore an important issue.

3. Single atoms confined in g-C_3N_4

Graphitic carbon nitride (g-C_3N_4) is one of the oldest synthetic polymers [43] and has a broad range of applications in photocatalysis [44,45], organocatalysis [46], and other areas [47]. Unlike graphene or heteroatom-doped graphene, which are typical zero-bandgap materials, 2D g-C_3N_4 is a typical polymeric semiconductor with an sp^2 π-conjugated system [48].

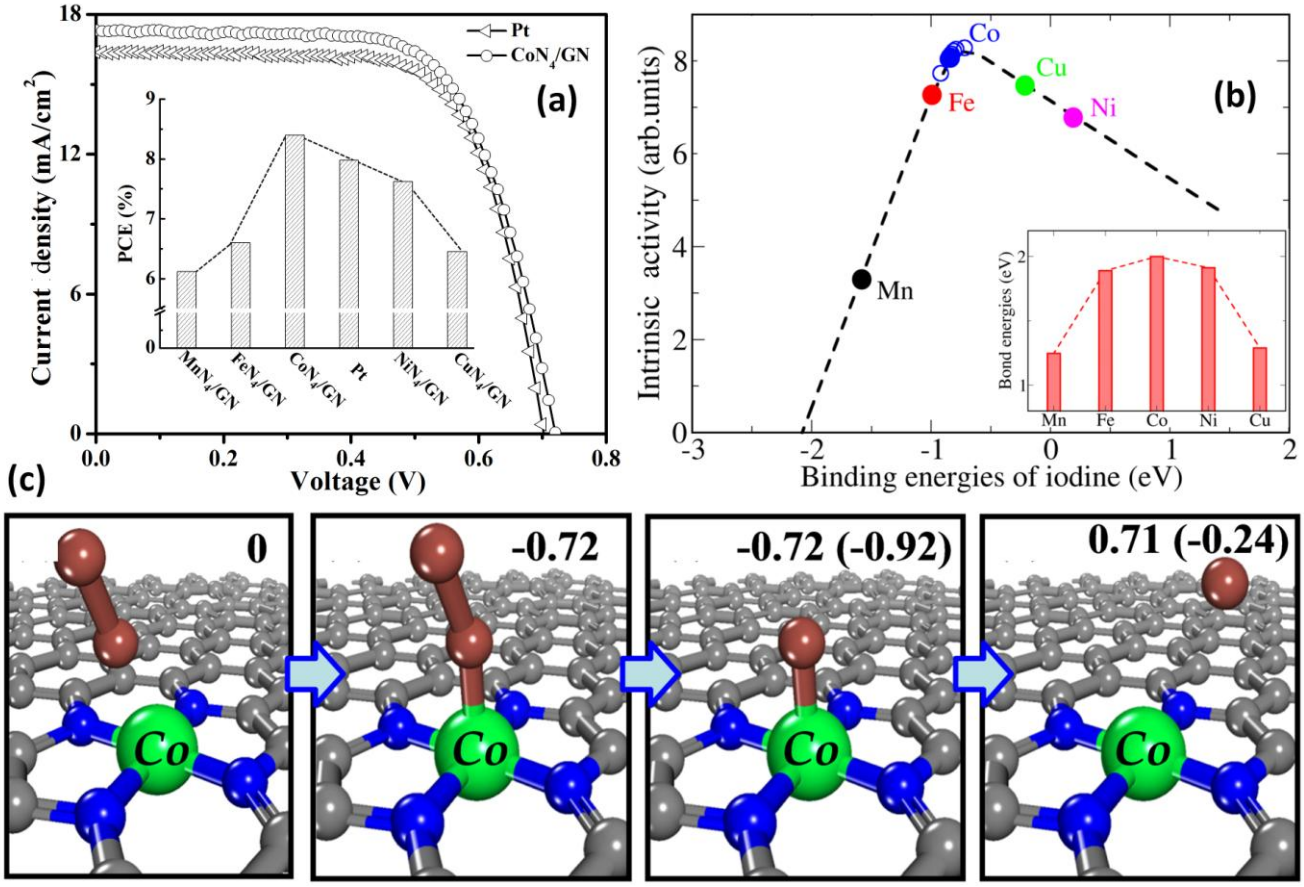

Fig. 5. (a) Current density voltage curves for DSSCs made from CoN_4/GN and Pt. Inset: measured PCEs of DSSCs fabricated with counter electrodes made from different MN_4/GNs and Pt [41]; (b) Intrinsic activity of MN_4/GN in triiodide reduction reaction on counter electrodes is denoted by filled circles, and open circles correspond to CoN_4/GN, taking solvent effects and charged states into account. Inset: stability of MN_4/GN structures in terms of M–N bond energies [41]; (c) Calculated energies of intermediates in triiodide reduction reaction on CoN_4/GN. Data in parentheses correspond to charged CoN_4/GN [41].

g-C_3N_4-confined SACs therefore have specific catalytic properties and applications [49–51]. Mesoporous g-C_3N_4 has the same microstructure as 2D g-C_3N_4, and is therefore also covered in this perspective [49,50].

Vile *et al*. [49] prepared a g-C_3N_4-confined Pd SAC for three-phase flow hydrogenation of alkynes and nitroarenes. Single Pd atoms were stabilized in the N-coordinating cavities through electrostatic interactions (Fig. 6(a)), which led to much higher activity, selectivity, and stability. In the selective hydrogenation of 1-hexyne, for example, the activity of Pd_1/g-C_3N_4 is an order of magnitude higher than that of the Lindlar catalyst at 90% selectivity to alkene, and its stability is good (Fig. 6(b)). DFT calculations showed that the high activity and selectivity can be attributed to facile hydrogen activation and alkyne adsorption on single Pd atoms. g-C_3N_4 is regarded as a special ligand for stabilizing single Pd atoms, inhibiting the adsorption of potential poisons (CO), and promoting H_2 activation.

Chen *et al*. [50] used a bottom-up strategy to synthesize a g-C_3N_4-confined Ag SAC via copolymerization of cyanamide with silver tricyanomethanide. The results showed single Ag atoms of valence state +1 in cages (Fig. 6(c)). In the semihydrogenation of 1-hexyne, the activity of Ag_1/g-C_3N_4 is about twice as high as those of Ag NP counterparts, and its selectivity is constant at 100% under a wide range of reaction conditions. It should be noted that such a bottom-up method can achieve much higher loadings of single metal atoms (10 wt% for Ag [50] and 8.5 wt% for Cu [35]) compared with those achieved using other common methods, by limiting the amount of metal to within 1 wt% to achieve single-atom dispersion.

Recently, Li *et al*. [51] reported that highly stable and dispersed isolated single Pt atoms anchored on 2D g-C_3N_4 can significantly enhance photocatalytic H_2 evolution activity. Its specific activity is 8.6 and 50 times higher than those of Pt NP-decorated g-C_3N_4 and bare g-C_3N_4, respectively. The N/C-coordinated framework formed by the tri-*s*-triazine structure facilitates the binding of single Pt atoms in the g-C_3N_4 matrix (Fig. 6(d)). It is proposed that these single Pt atoms change the surface trap states of g-C_3N_4, resulting in longer lifetimes of photogenerated electrons, leading to higher H_2 evolution activity. Unlike the above-mentioned single metal atoms whose properties are usually modified by supports, single Pt atoms used as a cocatalyst mainly modulate the electronic structure of g-C_3N_4, and therefore improve the photocatalytic performance [51].

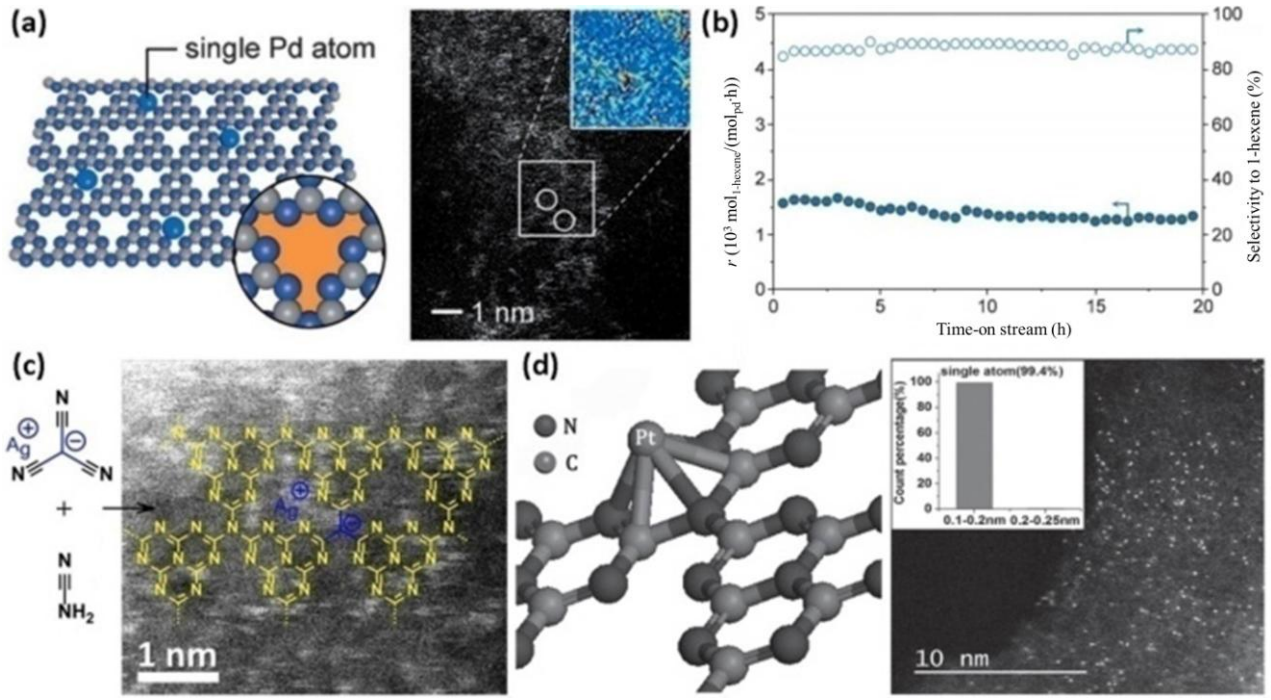

Fig. 6. (a) Structural configuration of $Pd_1/g\text{-}C_3N_4$ and corresponding HAADF-STEM image [49]; (b) Durability of $Pd_1/g\text{-}C_3N_4$ in selective hydrogenation of 1-hexyne at 70 °C and 0.5 MPa [49]; (c) Structural configuration of $Ag_1/g\text{-}C_3N_4$ and corresponding HAADF-STEM image [50]; (d) Structural configuration of $Pt_1/g\text{-}C_3N_4$ and corresponding HAADF-STEM image [51].

Research on $g\text{-}C_3N_4$-confined SACs is still in its infancy, especially in the case of 2D $g\text{-}C_3N_4$ [48]. Compared with N-doped graphene, a 2D $g\text{-}C_3N_4$ support has more specific N species and larger N-coordinating cavities for anchoring single metal atoms [52]. Most importantly, it is also a catalyst in itself, on which single metal atoms could stimulate its intrinsic nature in unusual ways. Such $g\text{-}C_3N_4$-confined SACs are expected to be excellent catalysts for various catalytic processes such as ORRs [53], oxygen evolution reactions [54], and photocatalytic reduction of CO_2 [55]. It is therefore an important challenge to achieve these energy-related aims and further expand the practical applications of these SACs.

4. Single atoms confined in MoS_2

Two-dimensional MoS_2 crystals, which have unusual physical and chemical properties, have been attracting increasing attention innumerous research fields during the past few years [14–16]. At present, there is a consensus that the active sites in MoS_2 correspond to coordinatively unsaturated S or Mo atoms along its edges [56–58], whereas the perfect in-plane domain of MoS_2 is always inert. Deng *et al.* [59] successfully activated the inert MoS_2 surface for HER catalysis by replacing Mo atoms with other single metal atoms. Among various transition metals, Pt is predicted to be the most effective for modulating the adsorption behavior of H atoms on neighboring S sites and consequently the HER activity (Fig. 7(a)). A one-pot solvothermal method was developed to achieve in-plane doping of single Pt atoms in 2D MoS_2. HAADF-STEM images (Fig. 7(c) and (d)) showed that the single Pt atoms (brighter white dots) were uniformly dispersed in the 2D MoS_2 plane and exactly occupied the positions of Mo atoms. Compared with pure few-layer MoS_2 (FL-MoS_2), Pt-doped 2D MoS_2 (Pt-MoS_2) showed significantly higher HER activity with a much lower overpotential (Fig. 7(b)). Moreover, its catalytic stability and poisoning resistance are superior to those of Pt supported on the 2D MoS_2 surface because of protection by the MoS_2 sandwich structure. This means that single Pt atoms do not directly catalyze the reduction of H_3O^+ but trigger HER activity of neighboring S atoms [59].

Fig. 7(a) also shows that Co is one of the best potential base metals for modulating the intrinsic activity of the MoS_2 surface, but the HER performance of Co-doped MoS_2 is greatly inferior to that of Pt-doped MoS_2 [59]. To improve the activities of such non-precious metal catalysts, Deng *et al.* [60] developed a multi-scale control strategy for constructing a 3D MoS_2-confined single Co atoms composite. Fig. 8(a) shows that the composite has uniform mesopores at the macroscale, which could facilitate the transport of H_3O^+ and H_2, and increase the accessibility of MoS_2 surface. At the nanoscale, oriented vertical growth of MoS_2 nanosheets around the mesopores increases the number of edges, which are active sites. At the atomic scale, chemical doping with single Co atoms of mesoporous MoS_2 foam (mPF-MoS_2) can further enhance the intrinsic HER activity by triggering the activity of neighboring S atoms. The authors also found that the optimum Co content in the Co doped mesoporous MoS_2 foam (mPF-Co-MoS_2) for high-performance HER activity was 16.7% (Fig. 8(b)); this material showed long-term durability over more than 5000 cycles and an overpotential of only 156 mV at a current density of 10 mV/cm², comparable to

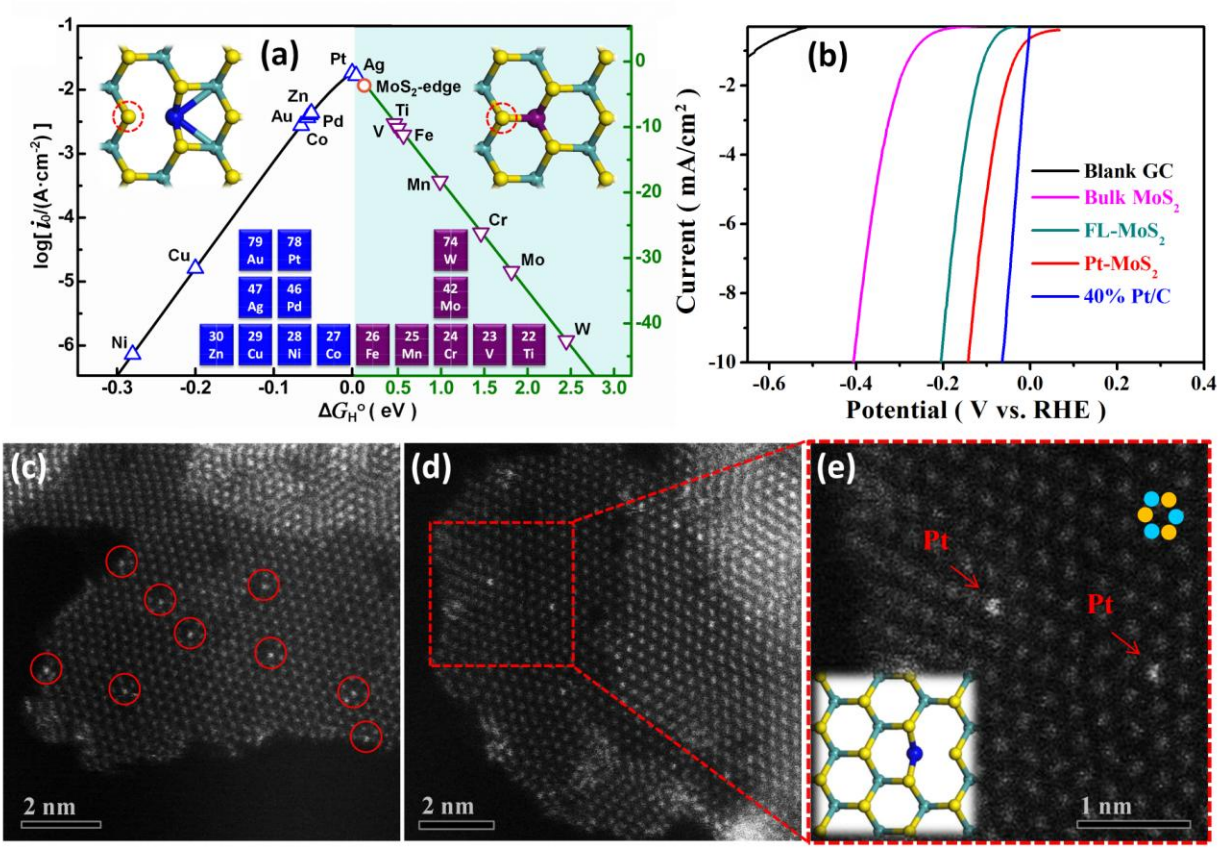

Fig. 7. (a) Relationship between current (logi_0) and difference in Gibbs free energy (ΔG_H^0) represented by volcano curve when 2D MoS_2 doped with single metal atoms used as catalyst [59]; (b) HER polarization curves for Pt-MoS_2, blank glassy carbon electrode, bulk MoS_2, FL-MoS_2, and 40% Pt/C [59]; (c–e) HAADF-STEM images of Pt-MoS_2 [59].

those of Pt-MoS_2 (Fig. 7(b)) and many other excellent MoS_2-based electrocatalysts. DFT calculations confirmed that moderate Co doping could modulate H adsorption on MoS_2 to a suitable degree and simultaneously maintain the structural stability, enabling the HER activity to reach the optimum value (Fig. 8(c)).

The above studies [59,60] explored the latent capacity of single metal atoms to trigger the intrinsic catalytic activity of the MoS_2 surface. This could equally be applied to other 2D transition-metal dichalcogenides (e.g., WS_2, $MoSe_2$, WSe_2, and $MoTe_2$). The potential influences of such inductive effects in 2D MoS_2-confined SACs on other catalytic reactions such as hydrodesulfurization [61,62] and syngas conversion to higher alcohols [63,64] are worth studying. Alternatively, substituting S atoms in MoS_2 with single non-metal atoms such as B, N, and P is another promising method for tuning electronic structures and consequently catalytic behaviors.

5. Summary and perspectives

Here, we have summarized recent progress in the synthesis and catalytic applications of single atoms confined in 2D materials and discussed their possible catalytic mechanisms. Three 2D materials, namely graphene, g-C_3N_4, and MoS_2, were discussed. Of these, graphene is the most studied and usually only serves as a support on which suitable types and numbers of main-group elements (e.g., C, N, O, and S) are essential for stabilizing single atoms and simultaneously maintaining their coordinatively unsaturated states for catalysis. g-C_3N_4 has abundant N species and large N-coordinating cavities for anchoring single metal atoms; its 2D heterostructures are still under development. Recently, a 2D C_2N material was successfully synthesized and characterized [65,66]. Its N content falls between those of regular N-doped graphene and g-C_3N_4, which should endow the supported single metal atoms with some unexpected catalytic activities.

Rather than the usual use of single atoms as active sites [8,9], this perspective emphasized the special role of single atoms in promoting the intrinsic catalytic properties of 2D materials, if the 2D materials themselves have catalytic abilities, e.g., g-C_3N_4 for photocatalysis [51] and MoS_2 for electrocatalysis [59,60]. Similarly to 2D transition-metal dichalcogenides [59, 60], 2D metal oxides (e.g., layered double hydroxides, TiO_2, and perovskite-type materials) [15] are efficient catalysts in various catalytic processes and have seldom been studied for the confinement of single atoms [67,68]. This is therefore a large and promising field of research on catalysis for energy and environmental science.

The mutual benefits between 2D materials and single atoms make their composites excellent models for developing real catalysts. Efficient methods for the synthesis of SACs confined in 2D materials, rather than just the preparation of such 2D

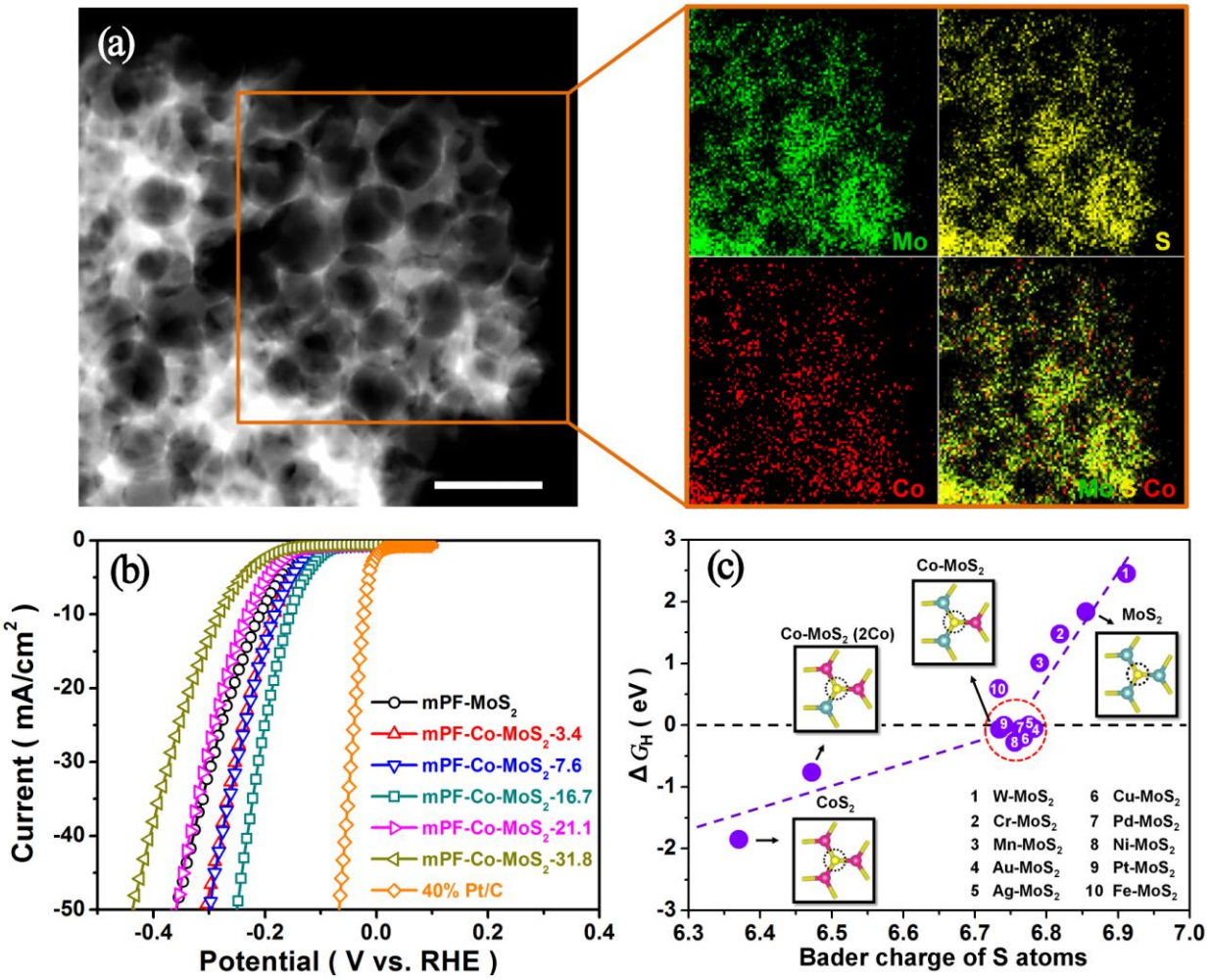

Fig. 8. (a) HAADF-STEM image of mPF-Co-MoS_2 and corresponding energy-dispersive X-ray maps. Scale bar: 100 nm [60]; (b) HER polarization curves form PF-Co-MoS_2 with various doped Co contents and those of mPF-MoS_2 and 40% Pt/C [60]; (c) ΔG_H of S atoms versus Bader charge of S atoms for different structures. Insets: atomic configurations of Co-MoS_2 with different atomic ratios of Co to Mo [60].

materials [69], is therefore important. Precise control of the structure can facilitate recognition of the real active sites in situ and can help to elucidate the catalytic mechanism objectively [70,71]. Furthermore, the mass production of 2D materials with confined high-density and highly dispersed SACs is necessary for practical applications. How to combine both aspects is an ongoing issue in this pioneering field and will undoubtedly have a far-reaching impact on fundamental research and industrial applications.

Acknowledgments

We gratefully acknowledge the financial support from the Ministry of Science and Technology of China (2016YFA0204100, 2016YFA0200200), the National Natural Science Foundation of China (21573220, 21621063), the Key Research Program of Frontier Sciences of the Chinese Academy of Sciences (QYZDB-SSW-JSC020), and the Strategic Priority Research Program of the Chinese Academy of Sciences (XDA09030100).

Dehui Deng
State Key Laboratory of Catalysis, Collaborative Innovation Center of Chemistry for Energy Materials (*i*ChEM), Dalian Institute of Chemical Physics, Chinese Academy of Sciences, Dalian 116023, Liaoning, China;
iChEM, College of Chemistry and Chemical Engineering, Xiamen University, Xiamen 361005, Fujian, China
Tel/Fax: +86-411-84379128
dhdeng@dicp.ac.cn

Xinhe Bao
State Key Laboratory of Catalysis, Collaborative Innovation Center of Chemistry for Energy Materials (*i*ChEM), Dalian Institute of Chemical Physics, Chinese Academy of Sciences, Dalian 116023, Liaoning, China
Tel: +86-411-84686637
Fax: +86-411-84379128
xhbao@dicp.ac.cn
Received 23 March 2017
Published 5 September 2017
DOI: 10.1016/S1872-2067(17)62839-0

References

[1] B. K. Burgess, D. J. Lowe, *Chem. Rev*., **1996**, 96, 2983–3011.
[2] W. Nam, *Acc. Chem. Res*., **2007**, 40, 522–531.
[3] J. R. Black, Q. Z. Yin, J. R. Rustad, W. H. Casey, *J. Am. Chem. Soc*., **2007**, 129, 8690–8691.
[4] M. Flytzani-Stephanopoulos, B. C. Gates, *Annu. Rev. Chem. Biomol. Eng*., **2012**, 3, 545–574.
[5] J. M. Thomas, R. Raja, D. W. Lewis, *Angew. Chem. Int. Ed*., **2005**, 44, 6456–6482.
[6] J. M. Thomas, Z. Saghi, P. L. Gai, *Top. Catal*., **2011**, 54, 588–594.
[7] B. T. Qiao, A. Q. Wang, X. F. Yang, L. F. Allard, Z. Jiang, Y. T. Cui, J. Y. Liu, J. Li, T. Zhang, *Nat. Chem*., **2011**, 3, 634–641.
[8] X. F. Yang, A. Q. Wang, B. T. Qiao, J. Li, J. Y. Liu, T. Zhang, *Acc. Chem. Res*., **2013**, 46, 1740–1748.
[9] J. Liu, *ACS Catal*., **2016**, 7, 34–59.
[10] X. G. Guo, G. Z. Fang, G. Li, H. Ma, H. J. Fan, L. Yu, C. Ma, X. Wu, D. H. Deng, M. M. Wei, D. L. Tan, R. Si, S. Zhang, J. Q. Li, L. T. Sun, Z. C. Tang, X. L. Pan, X. H. Bao, *Science*, **2014**, 344, 616–619.
[11] P. X. Liu, Y. Zhao, R. X. Qin, S. G. Mo, G. X. Chen, L. Gu, D. M. Chevrier, P. Zhang, Q. Guo, D. D. Zang, B. H. Wu, G. Fu, N. F. Zheng, *Science*, **2016**, 352, 797–801.
[12] J. Jones, H. F. Xiong, A. T. Delariva, E. J. Peterson, H. Pham, S. R. Challa, G. S. Qi, S. Oh, M. H. Wiebenga, X. I. P. Hernandez, Y. Wang, A. K. Datye, *Science*, **2016**, 353, 150–154.
[13] K. S. Novoselov, A. K. Geim, S. V. Morozov, D. Jiang, Y. Zhang, S. V. Dubonos, I. V. Grigorieva, A. A. Firsov, *Science*, **2004**, 306, 666–669.
[14] K. S. Novoselov, D. Jiang, F. Schedin, T. J. Booth, V. V. Khotkevich, S. V. Morozov, A. K. Geim, *P. Natl. Acad. Sci. USA*, **2005**, 102, 10451–10453.
[15] A. K. Geim, I. V. Grigorieva, *Nature*, **2013**, 499, 419–425.
[16] M. S. Xu, T. Liang, M. M. Shi, H. Z. Chen, *Chem. Rev*., **2013**, 113, 3766–3798.
[17] D. Deng, K. S. Novoselov, Q. Fu, N. Zheng, Z. Tian, X. Bao, *Nat. Nanotechnol*., **2016**, 11, 218–230.
[18] S. Back, J. Lim, N. Y. Kim, Y. H. Kim, Y. Jung, *Chem. Sci*., **2017**, 8, 1090–1096
[19] J. Duan, S. Chen, M. Jaroniec, S. Z. Qiao, *ACS Catal*., **2015**, 5, 5207–5234.
[20] L. K. Putri, W. J. Ong, W. S. Chang, S. P. Chai, *Appl. Surf. Sci*., **2015**, 358, 2–14.
[21] H. Wang, T. Maiyalagan, X. Wang, *ACS Catal*. **2012**, 2, 781–794.
[22] D. Deng, X. Pan, L. Yu, Y. Cui, Y. Jiang, J. Qi, W. X. Li, Q. Fu, X. Ma, Q. Xue, G. Sun, X. Bao, *Chem. Mater*., **2011**, 23, 1188–1193.
[23] L. Y. Zhao, R. He, K. T. Rim, T. Schiros, K. S. Kim, H. Zhou, C. Gutierrez, S. P. Chockalingam, C. J. Arguello, L. Palova, D. Nordlund, M. S. Hybertsen, D. R. Reichman, T. F. Heinz, P. Kim, A. Pinczuk, G. W. Flynn, A. N. Pasupathy, *Science*, **2011**, 333, 999–1003.
[24] S. Sun, G. Zhang, N. Gauquelin, N. Chen, J. Zhou, S. Yang, W. Chen, X. Meng, D. Geng, M. N. Banis, R. Li, S. Ye, S. Knights, G. A. Botton, T. K. Sham, X. Sun, *Sci. Rep*., **2013**, 3, 1775–1783.
[25] S. Stambula, N. Gauquelin, M. Bugnet, S. Gorantla, S. Turner, S. Sun, J. Liu, G. Zhang, X. Sun, G. A. Botton, *J. Phys. Chem. C*, **2014**, 118, 3890–3900.
[26] N. Cheng, S. Stambula, D. Wang, M. N. Banis, J. Liu, A. Riese, B. Xiao, R. Li, T. K. Sham, L. M. Liu, G. A. Botton, X. Sun, *Nat. Commun*., **2016**, 7, 13638.
[27] H. Wang, Q. Wang, Y. Cheng, K. Li, Y. Yao, Q. Zhang, C. Dong, P. Wang, U. Schwingenschlogl, W. Yang, X. X. Zhang, *Nano Lett*., **2012**, 12, 141–144.
[28] H. Yan, H. Cheng, H. Yi, Y. Lin, T. Yao, C. Wang, J. Li, S. Wei, J. Lu, *J. Am. Chem. Soc*., **2015**, 137, 10484–10487.
[29] H. J. Qiu, Y. Ito, W. Cong, Y. Tan, P. Liu, A. Hirata, T. Fujita, Z. Tang, M. Chen, *Angew. Chem. Int. Ed*., **2015**, 54, 14031–14035.
[30] L. Zhang, A. Wang, W. Wang, Y. Huang, X. Liu, S. Miao, J. Liu, T. Zhang, *ACS Catal*., **2015**, 5, 6563–6572.
[31] H. Fei, J. Dong, M. J. Arellano-Jimenez, G. Ye, N. D. Kim, E. L. Samuel, Z. Peng, Z. Zhu, F. Qin, J. Bao, M. J. Yacaman, P. M. Ajayan, D. Chen, J. M. Tour, *Nat. Commun*., **2015**, 6, 8668.
[32] D. A. Bulushev, M. Zacharska, E. V. Shlyakhova, A. L. Chuvilin, Y. Guo, S. Beloshapkin, A. V. Okotrub, L. G. Bulusheva, *ACS Catal*., **2016**, 6, 681–691.
[33] D. A. Bulushev, M. Zacharska, A. S. Lisitsyn, O. Y. Podyacheva, F. S. Hage, Q. M. Ramasse, U. Bangert, L. G. Bulusheva, *ACS Catal*., **2016**, 6, 3442–3451.
[34] M. Lefevre, E. Proietti, F. Jaouen, J. P. Dodelet, *Science*, **2009**, 324, 71–74.
[35] H. Wu, H. Li, X. Zhao, Q. Liu, J. Wang, J. Xiao, S. Xie, R. Si, F. Yang, S. Miao, X. Guo, G. Wang, X. Bao, *Energy Environ. Sci*., **2016**, 9,

Graphical Abstract

Chin. J. Catal., 2017, 38: 1443–1453 doi: 10.1016/S1872-2067(17)62839-0

Two-dimensional materials confining single atoms for catalysis

Yong Wang, Wenhua Zhang, Dehui Deng *, Xinhe Bao *
Dalian Institute of Chemical Physics, Chinese Academy of Sciences; Institute of Chemical Materials, China Academy of Engineering Physics; Xiamen University

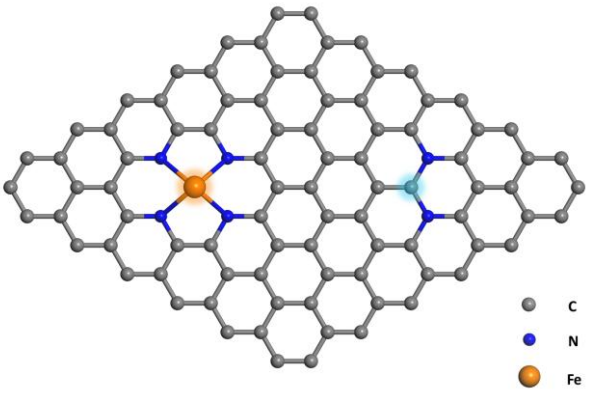

Two-dimensional materials confining single atoms, the mutually beneficial cooperation for highly efficient catalysis.

3736–3745.
[36] X. D. Yang, Y. P. Zheng, J. Yang, W. Shi, J. H. Zhong, C. K. Zhang, X. Zhang, Y. H. Hong, X. X. Peng, Z. Y. Zhou, S. G. Sun, *ACS Catal*., **2017**, 7, 139–145.
[37] W. Liu, L. Zhang, W. Yan, X. Liu, X. Yang, S. Miao, W. Wang, A. Wang, T. Zhang, *Chem. Sci*., **2016**, 7, 5758–5764.
[38] D. Deng, X. Chen, L. Yu, X. Wu, Q. Liu, Y. Liu, H. Yang, H. Tian, Y. Hu, P. Du, R. Si, J. Wang, X. Cui, H. Li, J. Xiao, T. Xu, J. Deng, F. Yang, P. N. Duchesne, P. Zhang, J. Zhou, L. Sun, J. Li, X. Pan, X. Bao, *Sci. Adv*., **2015**, 1, e1500462/1–e1500462/9.
[39] Q. Liu, Y. Liu, H. Li, L. Li, D. Deng, F. Yang, X. Bao, *Appl. Surf. Sci*., **2017**, 410, 111–116.
[40] X. Chen, L. Yu, S. Wang, D. Deng, X. Bao, *Nano Energy*, **2017**, 32, 353–358.
[41] X. Cui, J. Xiao, Y. Wu, P. Du, R. Si, H. Yang, H. Tian, J. Li, W. H. Zhang, D. Deng, X. Bao, *Angew. Chem. Int. Ed*., **2016**, 55, 6708–6712.
[42] C. H. Choi, M. Kim, H. C. Kwon, S. J. Cho, S. Yun, H. T. Kim, K. J. Mayrhofer, H. Kim, M. Choi, *Nat. Commun*., **2016**, 7, 10922.
[43] A. Thomas, A. Fischer, F. Goettmann, M. Antonietti, J. O. Muller, R. Schlogl, J. M. Carlsson, *J. Mater. Chem*., **2008**, 18, 4893–4908.
[44] X. C. Wang, S. Blechert, M. Antonietti, *ACS Catal*., **2012**, 2, 1596–1606.
[45] Y. Zheng, L. H. Lin, B. Wang, X. C. Wang, *Angew. Chem. Int. Ed*., **2015**, 54, 12868–12884.
[46] Y. Wang, X. C. Wang, M. Antonietti, *Angew. Chem. Int. Ed*., **2012**, 51, 68–89.
[47] J. Liu, H. Q. Wang, M. Antonietti, *Chem. Soc. Rev*., **2016**, 45, 2308–2326.
[48] J. S. Zhang, Y. Chen, X. C. Wang, *Energy Environ. Sci*., **2015**, 8, 3092–3108.
[49] G. Vile, D. Albani, M. Nachtegaal, Z. Chen, D. Dontsova, M. Antonietti, N. Lopez, J. Perez-Ramirez, *Angew. Chem. Int. Ed*., **2015**, 54, 11265–11269.
[50] Z. Chen, S. Pronkin, T. P. Fellinger, K. Kailasam, G. Vile, D. Albani, F. Krumeich, R. Leary, J. Barnard, J. M. Thomas, J. Perez-Ramirez, M. Antonietti, D. Dontsova, *ACS Nano*, **2016**, 10, 3166–3175.
[51] X. Li, W. Bi, L. Zhang, S. Tao, W. Chu, Q. Zhang, Y. Luo, C. Wu, Y. Xie, *Adv. Mater*., **2016**, 28, 2427–2431.
[52] Z. Chen, S. Mitchell, E. Vorobyeva, R. K. Leary, R. Hauert, T. Furnival, Q. M. Ramasse, J. M. Thomas, P. A. Midgley, D. Dontsova, M. Antonietti, S. Pogodin, N. López, J. Pérez-Ramírez, *Adv. Funct. Mater*., **2017**, 27, 1605785.
[53] F. He, K. Li, C. Yin, Y. Wang, H. Tang, Z. Wu, *Carbon*, **2017**, 114, 619–627.
[54] X. Li, P. Cui, W. Zhong, J. Li, X. Wang, Z. Wang, J. Jiang, *Chem. Commun*., **2016**, 52, 13233–13236.
[55] G. Gao, Y. Jiao, E. R. Waclawik, A. Du, *J. Am. Chem. Soc*., **2016**, 138, 6292–6297.
[56] P. G. Moses, B. Hinnemann, H. Topsoe, J. K. Norskov, *J. Catal*., **2007**, 248, 188–203.
[57] S. Zaman, K. J. Smith, *Catal. Rev*., **2012**, 54, 41–132.
[58] T. F. Jaramillo, K. P. Jorgensen, J. Bonde, J. H. Nielsen, S. Horch, I. Chorkendorff, *Science*, **2007**, 317, 100–102.
[59] J. Deng, H. Li, J. Xiao, Y. Tu, D. Deng, H. Yang, H. Tian, J. Li, P. Ren, X. Bao, *Energy Environ. Sci*., **2015**, 8, 1594–1601.
[60] J. Deng, H. Li, S. Wang, D. Ding, M. Chen, C. Liu, Z. Tian, K. S. Novoselov, C. Ma, D. Deng, X. Bao, *Nat. Commun*., **2017**, 8, 14430.
[61] J. V. Lauritsen, F. Besenbacher, *J. Catal*., **2015**, 328, 49–58.
[62] S. S. Grønborg, M. Šarić, P. G. Moses, J. Rossmeisl, J. V. Lauritsen, *J. Catal*., **2016**, 344, 121–128.
[63] M. Taborga Claure, S.-H. Chai, S. Dai, K. A. Unocic, F. M. Alamgir, P. K. Agrawal, C. W. Jones, *J. Catal*., **2015**, 324, 88–97.
[64] V. S. Dorokhov, E. A. Permyakov, P. A. Nikulshin, V. V. Maximov, V. M. Kogan, *J. Catal*., **2016**, 344, 841–853.
[65] J. Mahmood, E. K. Lee, M. Jung, D. Shin, I. Y. Jeon, S. M. Jung, H. J. Choi, J. M. Seo, S. Y. Bae, S. D. Sohn, N. Park, J. H. Oh, H. J. Shin, J. B. Baek, *Nat. Commun*., **2015**, 6, 6486.
[66] J. Mahmood, F. Li, S. M. Jung, M. S. Okyay, I. Ahmad, S. J. Kim, N. Park, H. Y. Jeong, J. B. Baek, *Nat. Nanotechnol*., **2017**, 12, 441–446.
[67] S. Ida, N. Kim, E. Ertekin, S. Takenaka, T. Ishihara, *J. Am. Chem. Soc*., **2015**, 137, 239–244.
[68] Y. Zhu, Z. An, J. He, *J. Catal*., **2016**, 341, 44–54.
[69] B. C. Gates, *J. Catal*., **2015**, 328, 72–74.
[70] B. T. Qiao, J. X. Liang, A. Q. Wang, J. Y. Liu, T. Zhang, *Chin. J. Catal*. **2016**, 37, 1580–1587.
[71] C. Li, *Chin. J. Catal*. **2016**, 37, 1443–1445.

二维材料限域单原子催化剂研究进展

王　勇[a,c], 张文华[b], 邓德会[a,c,*], 包信和[a,#]

[a]中国科学院大连化学物理研究所, 教育部能源材料化学协同创新中心, 催化基础国家重点实验室, 辽宁大连116023

[b]中国工程物理研究院化工材料研究所, 四川省新材料研究中心, 四川成都610200

[c]厦门大学化学化工学院, 教育部能源材料化学协同创新中心, 固体表面物理化学国家重点实验室, 福建厦门361005

摘要: 近年来, 单一原子或单一位点催化剂因其独特的结构和电子特性受到催化研究人员的广泛关注. 目前, 多种无机固体材料被用作限域该类单原子催化剂, 包括传统的金属氧化物、沸石分子筛以及金属有机框架配合物等. 载体的性质会显著地影响单原子的催化性能, 因此具有独特物理化学性质的二维材料无疑是限域单原子的一类理想介质, 并逐渐引起了人们在该领域的研究兴趣.

二维材料兴起于石墨烯的成功剥离, 随后其他类似物如氮化硼、氮化碳以及二硫化钼等蓬勃发展起来. 结构简单明确且性质独特的二维材料自身就是一类新颖的催化剂, 其与单原子的结合将会为催化带来更多新的可能. 二维材料限域单原子催化剂的潜在优势如下: (1)二维材料独特的电子结构对单原子中心的电子特性有显著的调变作用, 使其催化性能更为独特; (2)二维材料通常具有巨大的比表面积, 这允许其锚定更多的单原子从而显著提高其活性位密度; (3)单原子层二维材料有利于反应物分子从双向接触其表面限域的单原子位点, 增加碰撞几率并降低传质阻力; (4)二维材料限域单原子催化剂可被视为理想的模型催化剂, 其结构均一的活性中心有利于催化剂构效关系的研究; (5)二维材料限域的单原子能够反过来促进或激活二维材料的本征催化活性.

在这里, 我们总结了二维材料限域单原子催化剂的最新进展, 其中二维材料主要涉及石墨烯、氮化碳和硫化钼. 我们围绕在二维材料限域单原子催化剂中什么是真正的活性位点及其如何协同催化等问题进行了讨论, 进而展望了二维材料限域单原子催化剂的应用前景和挑战.

关键词: 二维材料; 单原子催化剂; 石墨烯; 石墨烯类似物; 氮化碳; 硫化钼

收稿日期: 2017-03-23. 接受日期: 2017-04-13. 出版日期: 2017-09-05.

*通讯联系人. 电话/传真: (0411)84379128; 电子信箱: dhdeng@dicp.ac.cn

#通讯联系人. 电话: (0411)84686637; 传真: (0411)84379128; 电子信箱: xhbao@dicp.ac.cn

基金来源: 科技部国家重点研发计划(2016YFA0204100, 2016YFA0200200); 国家自然科学基金(21573220, 21621063); 中国科学院前沿科学重点研究计划(QYZDB-SSW-JSC020); 中国科学院战略性先导科技专项(XDA09030100).

本文的英文电子版由Elsevier出版社在ScienceDirect上出版(http://www.sciencedirect.com/science/journal/18722067).